energies

MDPI

Article

Application of the Salp Swarm Algorithm to Optimal Design of Tuned Inductive Choke

Łukasz Knypiński *, Milena Kurzawa, Rafał Wojciechowski and Michał Gwóźdź

Institute of Electrical Engineering and Electronics, Poznan University of Technology, Piotrowo 3A, 60-965 Poznan, Poland; milena.kurzawa@put.poznan.pl (M.K.); rafal.wojciechowski@put.poznan.pl (R.W.); michal.gwozdz@put.poznan.pl (M.G.)

* Correspondence: lukasz.knypinski@put.poznan.pl; Tel.: +48-61-665-2636

Abstract: The article presents an algorithm and optimization software designed for the optimal configuration of a tuned inductive choke. The optimization software consists of two main parts: an optimization procedure and a mathematical model for the designed electromagnetic devices. A lumped-parameters model of a tuned inductive choke was developed, with the device's structure described by three design variables. As an optimality criterion, the multi-objective compromise function was adopted. The objective function merges the total inductances of the electromagnetic device under different operation states. The optimized structure was analyzed using the finite element method. The developed lumped-parameters model is characterized by good accuracy and can be successfully applied to optimize tuned inductive chokes for various rated parameters. The optimization procedure was adapted to the tuned inductive choke model by appropriately selecting the characteristic coefficient of the salp swarm algorithm. The reliability of the optimization software was verified through experimental measurements.

Keywords: optimal design; multi-objective optimization; salp swarm algorithm; electromagnetic devices; lumped-parameters model; finite element method

Citation: Knypiński, Ł.; Kurzawa, M.; Wojciechowski, R.; Gwóźdź, M. Application of the Salp Swarm Algorithm to Optimal Design of Tuned Inductive Choke. *Energies* **2024**, *17*, 5129. https://doi.org/10.3390/en17205129

Academic Editors: Dan-Cristian Popa and Emil Cazacu

Received: 14 September 2024
Revised: 9 October 2024
Accepted: 13 October 2024
Published: 15 October 2024

1. Introduction

In the contemporary design process of electromagnetic devices, techniques utilizing the Finite Element Method (FEM) are commonly employed [1,2]. FEM allows for the accurate determination of field distribution within the designed device, as well as the precise calculation of its functional parameters [3]. Designers, drawing on their experience and intuition, initially select dimensions for which calculations are iteratively performed by varying individual variables to solve the analysis task. Following this, simulation calculations are conducted to analyze different specified parameters that describe the structure of the electromagnetic device under consideration [4,5].

By performing simulations for a series of selected structures, the designer aims to identify structural parameters that yield satisfactory functional outcomes for the designed device [6,7]. Conversely, during the synthesis process, known as optimal design, structural parameters are determined using an optimization algorithm. This algorithm automatically searches for the structural parameters that meet the imposed criteria by iteratively adjusting variables according to established rules [8,9].

Currently, the most widely used optimization algorithms are non-deterministic or heuristic algorithms [10]. These algorithms are particularly well-suited for optimizing devices described by both lumped parameter models, which are less computationally intensive, and more complex mathematical models developed using FEM [11,12].

A large and growing number of heuristic algorithms are available today, with new methods continually being developed. Recently, a significant group of methods, inspired by observations of groups of individuals in natural environments (nature-inspired algorithms), has gained prominence [13].

Heuristic algorithms include classical algorithms such as genetic algorithms and particle swarm optimization, which offer good convergence and a high probability of finding the global optimum. These methods are well-established and have been successfully applied to various optimization problems. However, newer algorithms, such as the grey wolf optimizer, the salp swarm algorithm, the sparrow search algorithm [14], and even the chimp optimization algorithm [15,16], are increasingly being utilized.

The aim of this paper is to develop a mathematical model, specifically a lumped parameter model based on the theory of magnetic circuits, for a variable, tunable inductive choke [17], and to perform optimization using a selected heuristic optimization algorithm, the Salp Swarm Algorithm (SSA).

Metaheuristic optimization algorithms very often require an appropriate selection of meta-parameters (adaptation) taken into account in mathematical model of the optimization algorithm [18]. In this paper, the authors adapted the optimization algorithm by appropriately selecting the coefficient a_1 of the SSA.

In the literature, there is no approach presenting the application of metaheuristic optimization algorithms to the optimal design of the tuned inductive chokes. In [19], the analytic model to design a three-phase compensation choke is employed. The iterative design process consists of changing selected structural parameters. In [20], the analytical design procedure to design choke inductors is presented.

This paper is organized as follows: Section 1 provides an introduction and literature review. The developed mathematical model of a tuned inductive choke is introduced in Section 2. In Section 3, the salp swarm optimization algorithm is described. The formulation of the optimization task is presented in Section 4. Furthermore, the results of the optimization calculation are demonstrated in Section 5. The results of simulation verification using the 3D FEM and experimental verification model are presented in Section 6. Lastly, a summary of the key findings and concluding remarks are given in Section 7.

2. Mathematical Model of a Tuned Inductive Choke

In this paper, the authors undertook the optimization of a variable, adjustable inductive choke, the construction of which was proposed in [13]. The primary focus of the choke design optimization was the appropriate selection of the air gaps in the choke system (Figure 1a) and the number of turns in the three coils used in the choke—namely, the main coil and two control coils. Detailed information about the choke's design and control method is provided in [17]. For the optimization process, the authors developed an Equivalent Lumped Parameter (ELP) model of the choke, based on the theory of magnetic circuits. The equivalent scheme of the choke, depicting the system of mutually interconnected reluctances, is shown in Figure 1b. The reluctances highlighted in yellow on the schematic represent those related to the areas with the magnetic core of the choke. The reluctances marked in green correspond to the flux leakages in the region of the individual choke coils, while the reluctances marked in blue are located in the air gap areas.

In order to determine the values of the individual reluctances assigned to specific sections of the core, the classical formula for calculating reluctance was used, i.e., the following relationship was applied:

$$R_{\mu i} = \frac{l_i}{\mu_o \mu_r S_i}, \tag{1}$$

where: l_i is the length of i-th fragment of the magnetic circuit of the choke, S_i is the cross-sectional area of the i-th section of the magnetic circuit; while μ_o and μ_r represent the magnetic permeability of air and the relative magnetic permeability, respectively.

To determine the reluctance values describing the path of the leakage flux in the region of each coil of the analyzed choke, the formula proposed in [21] was applied, i.e.,

$$R_{li} = \frac{h_{ri}}{\mu_o D_{wi} C_{wi} K_{Ri}}, \tag{2}$$

where: h_{ri} is the height of the i-th winding of the choke, D_{wi} is the distance between the given i-th winding and the core column of the inductor, C_{wi} is the average value of the circuit of the i-th winding, while K_{Ri} represents the Rogowski coefficient [22].

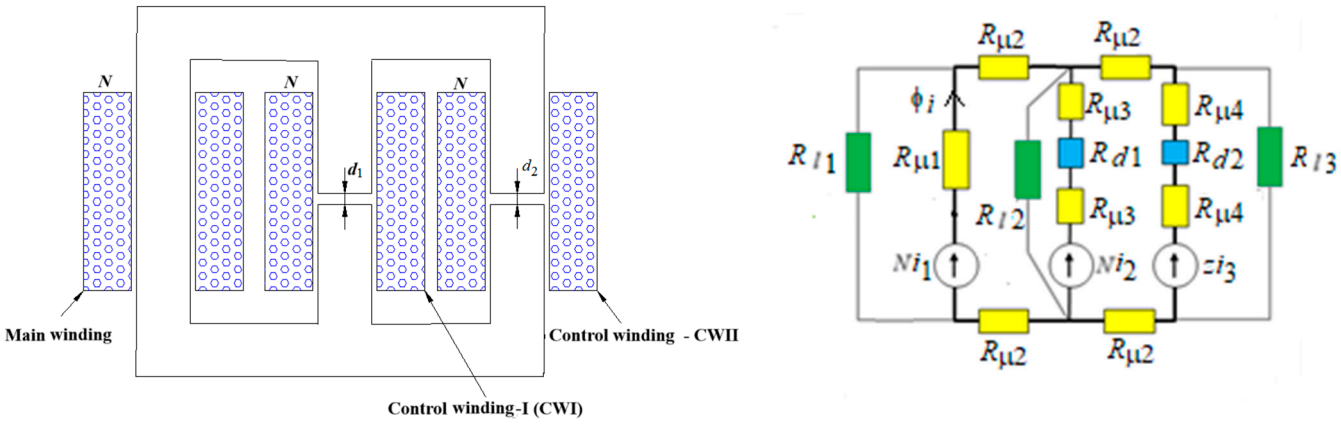

(**a**) (**b**)

Figure 1. (**a**) View of the tuned inductive choke structure, (**b**) lumped parameter tuned inductive choke.

In determining the reluctance values describing the air gap areas of the columns in the analysed inductor, the authors utilized the approach proposed by Schwarz–Christoffel [16]. In this approach, the reluctance value R_{di} of the considered air gap depends, among other factors, on the location of the gap within the column area (i.e., whether the gap is symmetrical with respect to the upper and lower yokes), the width w_c and depth h of the column, the height of the air gap l_a, and whether the column is located in the outer or central part of the magnetic circuit. Moreover, the Schwarz–Christoffel approach allows for the consideration of field distribution irregularities in gaps with a large l_a value. In the system analyzed in this work (Figure 1a), the working gaps were placed in the central column and the right outer column. In the Schwarz–Christoffel method, the reluctance value R_{di} of a given air gap is calculated as the parallel connection of two reluctance components (Figures 2 and 3). Therefore, in this approach, the reluctance value R_{d1} of the gap in the central column will be the parallel connection of two reluctances (Figure 2), calculated according to the following relation:

$$R'_g = \frac{1}{\mu_o h\left[\frac{w_c}{2l_a} + \frac{1}{\pi}\cdot\left(1 + ln\frac{\pi(c_c - w_c)}{2l_a}\right)\right]} \tag{3}$$

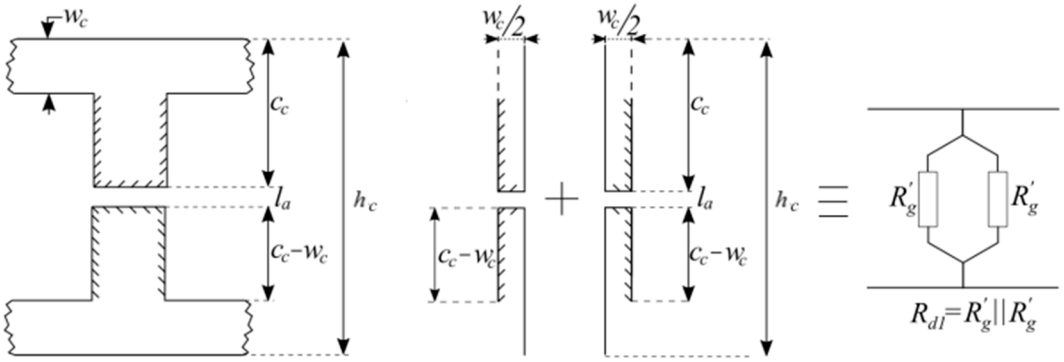

Figure 2. Visualization of the air gap in the area of the central column of the inductor from Figure 1a.

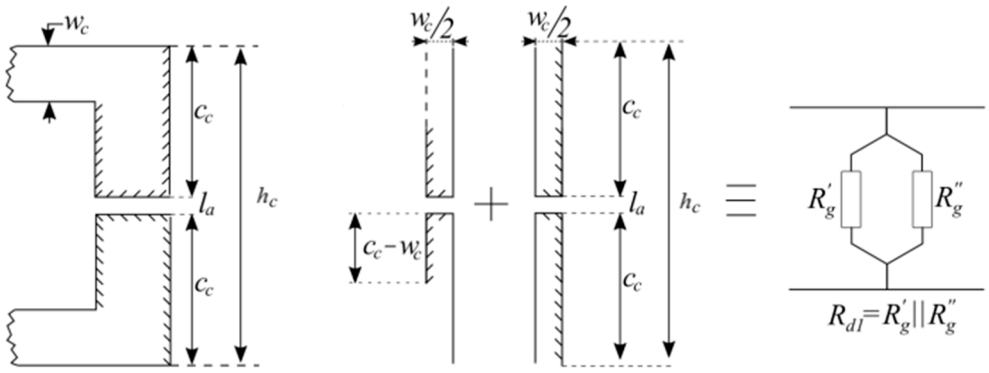

Figure 3. Visualization of the air gap in the area of the right outer column if the inductor from Figure 1a.

While the value of R_{d2} for the gap in the outer column (Figure 3), was calculated as the parallel connection of the reluctances R_g'—Equation (3)—and R_g''—Equation (4).

$$R_g'' = \frac{1}{\mu_o h\left[\frac{w_c}{2l_a} + \frac{1}{\pi}\cdot\left(1 + ln\frac{\pi c_c}{2l_a}\right)\right]}, \tag{4}$$

The values used in Equations (3) and (4) are presented in Figures 2 and 3.
The air gap reluctances for the second column are calculated using the formula:

$$R_{d1} = \frac{R_g' R_g'}{R_g' + R_g'}. \tag{5}$$

The air gap reluctances for the third column are determined:

$$R_{d2} = \frac{R_g' R_g''}{R_g' + R_g''}. \tag{6}$$

The primary factor subject to optimization in the considered system is primarily the inductance ratio for different configurations of control winding activation. Depending on the configuration (on/off) of the control windings in the inductor, four possible configurations result in four different inductance values, marked as L_1, L_2, L_3, and L_4. Where "switching on" a winding refers to connecting (short circuiting) the ends of the winding, while the winding is considered "switched off" when its ends remain open [13]. The winding configurations corresponding to each inductance value are summarized in Table 1.

Table 1. The dependence of inductance value on the configuration of the control windings.

Inductance of the Main Winding	Control Winding I	Control Winding II
L_1	switched off	switched off
L_2	switched on	switched off
L_3	switched off	switched on
L_4	switched on	switched on

In the developed approach, the inductance value was calculated from the definition:

$$L_i = \frac{\psi_i}{i_1} = \frac{N\phi_i}{i_1}, \tag{7}$$

where: ψ_i is the flux linkage with the main winding of the choke in the i-th configuration of the control winding, i_1 is the predetermined value of the current in the main winding, ϕ_i is

the magnetic flux in the column of the main winding of the magnetic circuit, and N is the number of turns in the main winding (it is assumed in the design that the number of turns in the control windings will also be N). The choke values were calculated using the loop method based on the equivalent circuit, assuming that when a given control winding is activated; the magnetomotive force of that winding will be equal to the magnetomotive force of the main winding.

3. Salp Swarm Optimization Algorithm

The salpid algorithm was developed in 2017 by Mirjalili [23], drawing inspiration from the behavior of salpids, a type of marine organism in the Thaliacea class. These creatures are known for forming large colonies, most often moving in chain formations. Salpids inhabit equatorial and cold waters. Their most numerous communities occur near Antarctica. Salpids move using contraction and pumping water through their gelatinous body, which is an example of one of the most efficient ways of moving in nature.

The Salp Swarm Algorithm (SSA) can be classified as a swarm intelligence method, but the latest research shows a high convergence of the method in comparison to the classical particle swarm algorithm [24,25].

The mathematical model of the optimization method was developed based on the social interactions that occurred in sapling colonies while searching for food. The method assumes that a chain consisting of all individuals forming a population follows the leader [26,27].

Salp population moves in a d-dimensional permissible area and the positions of all salps are described by the following matrix:

$$\mathbf{z} = \begin{bmatrix} z_1^1 & z_2^1 & \cdots & z_d^1 \\ z_1^2 & z_2^2 & \cdots & z_d^2 \\ & & & \\ z_1^m & z_2^m & & z_d^m \end{bmatrix}, \tag{8}$$

in which: $m = 1, 2, 3, \ldots, M$ is the salp number, M is the number of salps constituting the population.

The first stage of the optimization algorithm is the initialization of the initial population. In the developed algorithm, the starting population is created randomly. The population follows the food source, which is assumed to be the global extremum. In the SSA, the food source is assumed to be the position of the best-adapted individual creating the chain [28]. Then, the salp population is evaluated and ordered so that the best-adapted salp takes the first position in the matrix [29,30].

The position of the i-th individual (z^i) with the second highest value of the objective function in the swarm is determined:

$$\mathbf{z}^i = \begin{cases} \mathbf{S} + a_1[a_2(\mathbf{z}_{max} - \mathbf{z}_{min}) + \mathbf{z}_{min}] & \text{for } a_3 \geq 0 \\ \mathbf{S} + a_1[a_2(\mathbf{z}_{max} - \mathbf{z}_{min}) + \mathbf{z}_{min}] & \text{for } a_3 < 0' \end{cases} \tag{9}$$

where: $\mathbf{S}$ is the position of the best-adapted salp, a_1, a_2 are random numbers selected from the range (0, 1), $\mathbf{z}_{min}$, $\mathbf{z}_{max}$ are vectors of upper and lower values of decision variables.

The value of the characteristic coefficient a_1 is changed during the optimization process. In the k-th iteration, the value of the coefficient is determined according to equation:

$$a_1 = 2e^{-\left(\frac{5k}{2k_{max}}\right)}, \tag{10}$$

where: k_{max} is the maximum iteration number of iterations declared before starting the optimization process.

The new position of the i-th salp in the k-th iteration is calculated as follows:

$$\mathbf{z}_k^i = \frac{1}{2}\left(\mathbf{z}_k^i + \mathbf{z}_k^{i-1}\right), \tag{11}$$

The solution to Equation (9) requires the consideration of Newton's dynamics equation:

$$\mathbf{z}_k^i = \frac{1}{2}b(\Delta t)^2 + v\Delta t, \tag{12}$$

where: Δt is the time step, $b = v_f/v_0$, v_0 is the initial velocity, v_f is the final velocity.

The block diagram of salp swarm algorithm is presented in Figure 4.

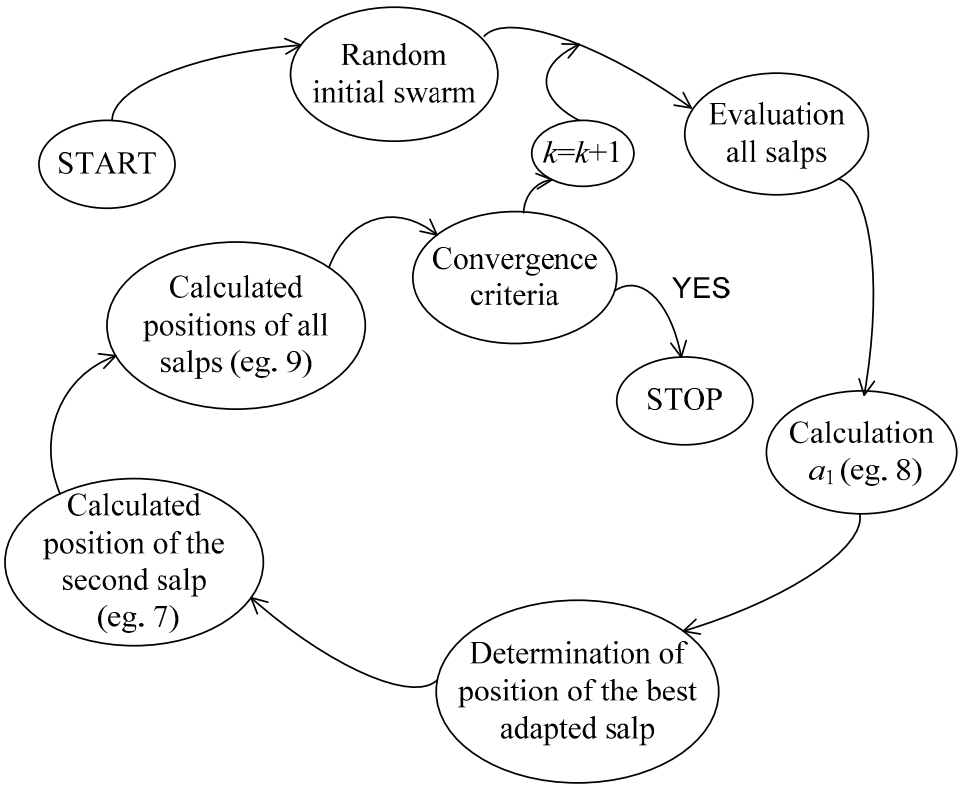

Figure 4. The flow chart of the elaborated SSA.

4. Formulation of the Optimization Task

The choke structure is described using three design variables: (a) d_1 is the air gap length of the middle choke column, (b) d_2 is the air gap length of the right choke column, and (c) N is the number of turns of each of the three-choke winding. All design variables form the vector $\mathbf{z} = [d_1, d_2, N]^T$. The ranges of variation of the decision variables are shown in Table 2.

Table 2. Ranges of variability of the design variables.

Design Variable	Upper Limit	Lower Limit
d_1 [mm]	3	8
d_2 [mm]	1	6
N	50	100

The choke with tuned inductance value, depending on the coil connection configuration, should provide the following total inductance values: $L_2 = 0.75L_1$, $L_3 = 0.5L_1$, $L_4 = 0.25L_1$.

After performing many optimization test runs for different variants involving the optimality criterion, the best repeatability of the final result was obtained for the following multi-objective function:

$$f(\mathbf{z}) = \lambda_1\left|\frac{L_2}{L_1} - 0.75\right| + \lambda_2\left|\frac{L_3}{L_1} - 0.5\right| + \lambda_3\left|\frac{L_4}{L_1} - 0.25\right|, \tag{13}$$

where: λ_1, λ_2, λ_3 are the weighting coefficients.

5. Results of the Optimization Calculations

Optimization calculations were performed for a chain consisting of 300 individuals (salps). The maximum value of the iterations (k_{max} = 30) was assumed as a stop criterion. The value of the weighting coefficients: λ_1 = 2, λ_2 = 2 and λ_3 = 1.5 were assumed. The optimization procedure was run 25 times. From all runs of the optimization procedure, the best, worst, and average values of the objective function and standard deviation were determined.

Table 3 summarizes the values of the design variables, particular inductances and the objective function value in the selected iterations of the optimization process, which ended with the lowest objective function value among the 25 analyzed processes.

Table 3. The course of the optimization process for the selected iteration of the optimization algorithm.

k	d_1 [mm]	d_2 [mm]	N	L_1 [mH]	L_2 [mH]	L_3 [mH]	L_4 [mH]	$f(z)$
1	5.903	1.919	64	6.458	5.201	2.861	1.531	0.03105035
2	6.107	1.926	81	4.956	3.774	2.478	1.239	0.02527294
4	6.104	1.925	82	5.083	3.872	2.542	1.271	0.02395790
8	6.114	1.924	81	4.956	3.775	2.478	1.270	0.02361123
10	6.115	1.925	81	4.957	3.776	2.478	1.239	0.02352791
15	6.115	1.926	81	4.958	3.776	2.479	1.239	0.02350626
20	6.115	1.926	81	4.959	3.775	2.478	1.238	0.02350527
25	6.115	1.926	81	4.959	3.775	2.478	1.238	0.02350522
30	6.115	1.926	81	4.959	3.775	2.478	1.238	0.02350522

Based on the results presented in Table 3, it can be concluded that during the first 10 iterations the optimization algorithm searched the permissible area, and the optimal solution was determined after 11 iterations of the optimization procedure.

Figure 5 shows a comparison of the convergence curves for the optimization process ending with the best value of the objective function value (green) and the optimization process ending with the worst value objective function value (red).

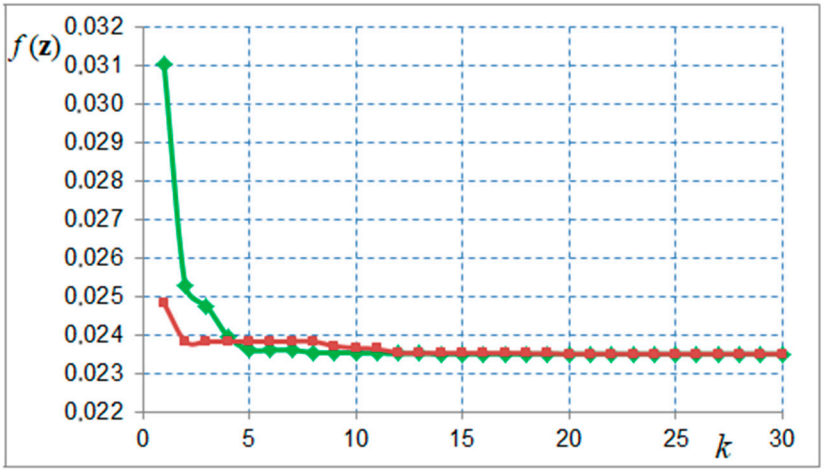

Figure 5. Comparison of the convergence curves for the optimization process with the best and worst values of the objective function.

The changes in values of inductances L_1, L_2, L_3 and L_4 during the optimization process are presented in Figure 6.

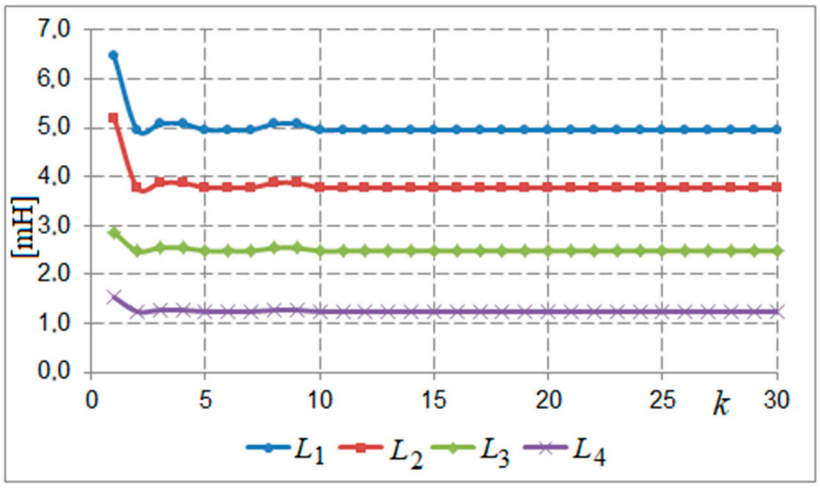

Figure 6. The convergence curves for L_1, L_2, L_3 and L_4.

The changes of the value of design variables d_1 and d_2 during optimization process are presented in Figure 7.

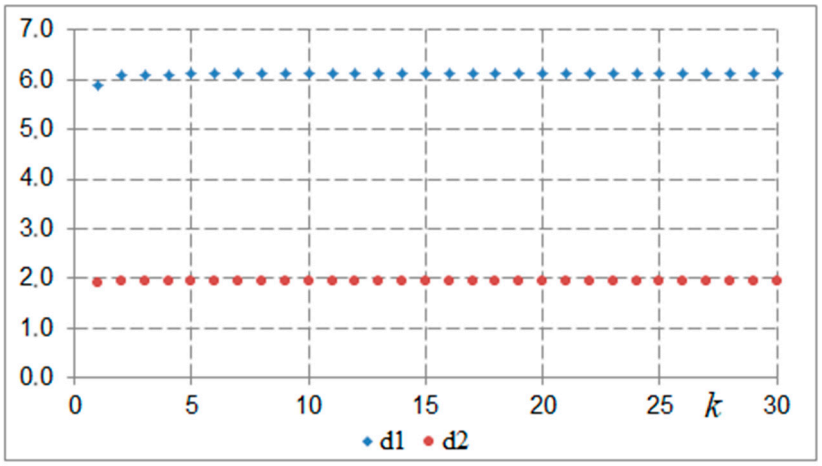

Figure 7. The convergence curves for d_1 and d_2.

It can be noted that the result close to the optimal one was determined after five iterations of the salp swarm algorithm. The optimal inductance values (the best results from 25 start optimization procedure) were obtained: L_1 = 4.959 mH, L_2 = 3.775 mH, L_3 = 2.478 mH and L_4 = 1.238 mH.

A statistical analysis was performed based on the results obtained during the series of optimization computations. The following values were determined: minimum value of the objective function, maximum value of the objective function, average value of the objective function from the analyzed series of simulation calculations and the standard deviation (SD).

The results of the statistical analysis are presented in Table 4. In all the analyzed optimization processes, the same values of the decision variables d_1 = 6.115 mm and d_2 = 1.926 mm were obtained. There were differences in the value of the number of turns in the winding (N) for selected optimization processes. Therefore, the results for the variable N were also added to Table 4.

Table 4. Statistical analysis for a series of optimization calculations.

	Minimum	**Maximum**	**Mean Value**	**SD**
$f(\mathbf{z})$	0.02350522	0.02350562	0.02350535	0.000000052
N	79	83	81.534	0.990430302

The results of the statistical analysis show that in the case of the optimized objective function, the value of the standard deviation is very small. Each time, the optimization process ends with a similar value of the objective function. The elaborated optimization procedure based on the salp swarm algorithm with adapted to solve optimization task a_1 characteristic coefficient is effective. However, the differences occur in the "optimal" values of the coil turns placed on the columns of the tuned induction coil.

6. Simulation and Experimental Verification of the Optimization Results

Simulation verification of the optimization results using 3D finite element calculations of the tuned inductive choke in the CST Studio Suite was executed. The structure of the tuned inductive choke was elaborated on the basis of optimization results.

The simulation model of the designed device in the CST Studio Suite environment is presented in Figure 8.

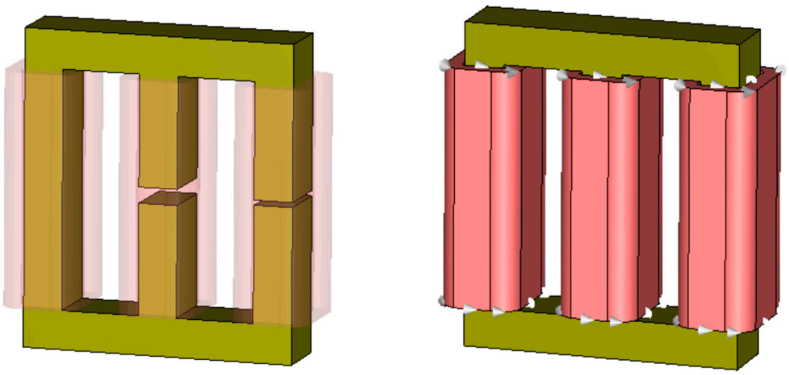

(**a**) (**b**)

Figure 8. The elaborated 3D model of tuned inductive choke: (**a**) view of the core with two air gaps in columns with transparent windings, (**b**) view of the full model.

Field computations were performed for various control winding configurations. The 3D field calculations for the steady-state operation were performed. The device was supplied by AC voltage with the parameters: maximum voltage U_{m} = 6 V and frequency f = 50 Hz. Figures 9–12 show the results of the electromagnetic field distribution in the designed tuned inductive choke for different operation states.

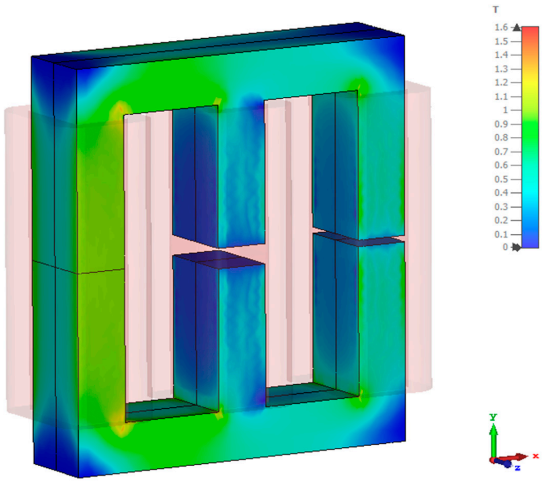

Figure 9. Distribution of the magnetic flux density vector for the operation state in which the current value in the main winding is maximum (I_m = 4.2 A), control winding I and control winding II are switched off.

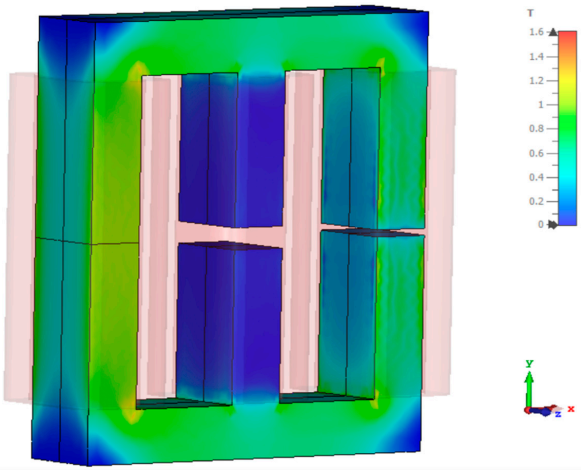

Figure 10. Distribution of the magnetic flux density vector for the operation state in which the current value in the main winding is maximum (I_m = 4.77 A), control winding I is switched on and control winding II is switched off.

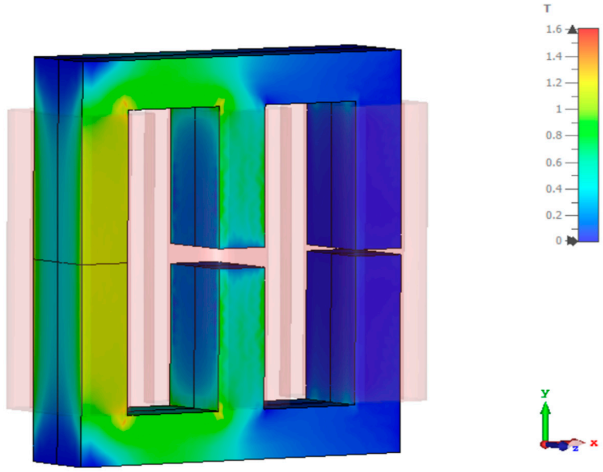

Figure 11. Distribution of the magnetic flux density vector for the operation state in which the current value in the main winding is maximum (I_m = 6.57 A), control winding I is switched off and control winding II is switched on.

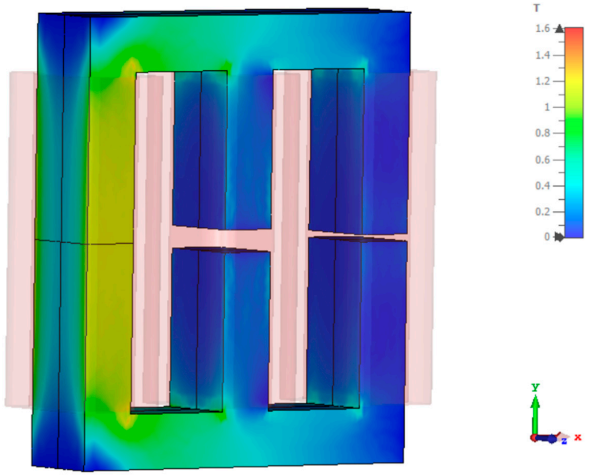

Figure 12. Distribution of the magnetic flux density vector for the operation state in which the current value in the main winding is maximum (I_m = 6.57 A), both control windings are switched on.

Next, a series of FEM calculations were made for different supply voltages. Such investigation should assess the suitability of the developed algorithm for designing a series of products allowing for the elimination of higher harmonics in the power network and power electronics systems.

The inductance values L_1, L_2, L_3 and L_4 for different supply voltages determined by simulation calculations are shown in Figure 13.

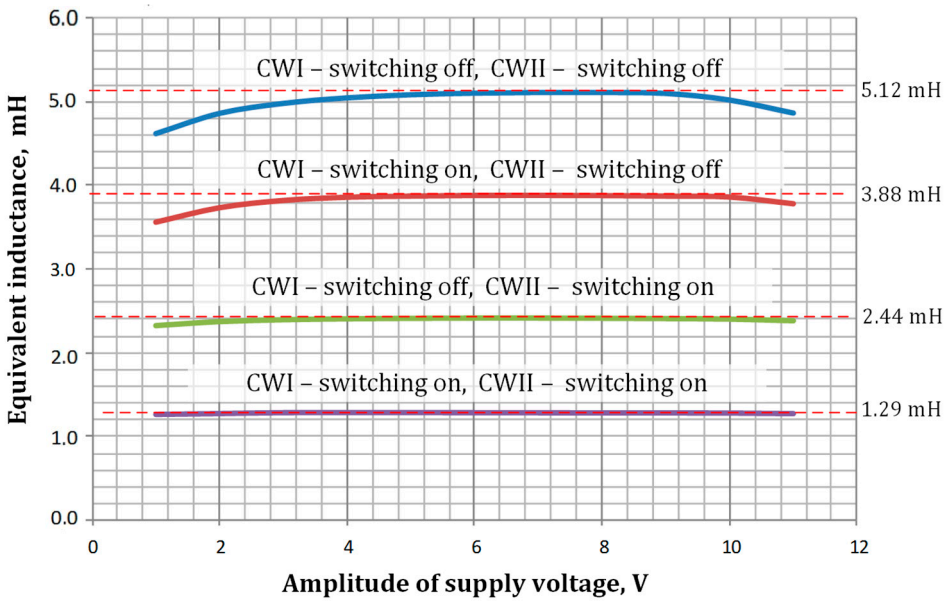

Figure 13. The 3D simulation results for different supply voltages, CWI—control winding I, CWII—control winding II.

The prototype of the tuned inductive choke was built based on the results of the optimization calculations. The view of the test stand with a three-phase choke prototype is presented in Figure 14. Figure 14 presents the three-phase tuned inductive choke prototype in the operation state in which the main winding is supplied, control winding I (CWI) is switched on and control winding II (CWII) is switched off.

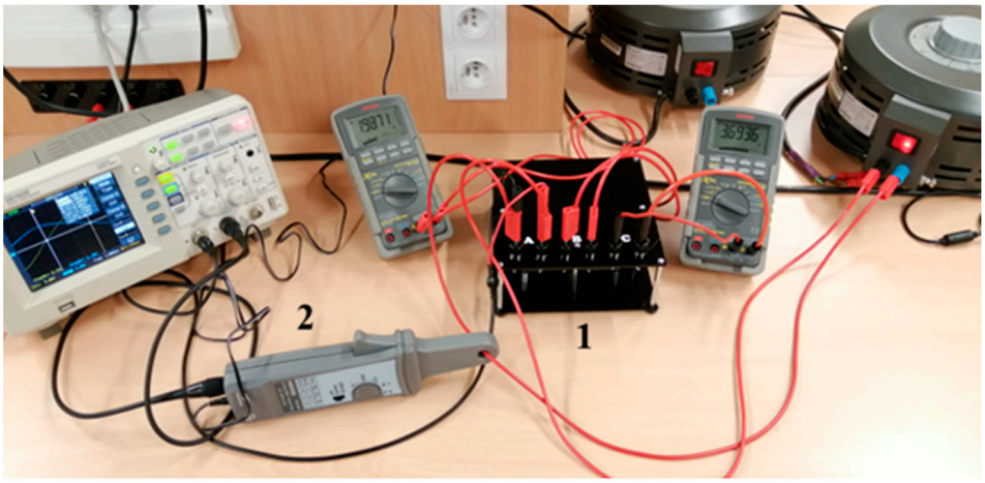

Figure 14. Experimental stand, 1—tuned inductive choke prototype, 2—clamp meter.

Next, experimental measurements of the prototype are executed for different supply voltage values. The main purpose of the performed series of measurements was to verify the accuracy of ratios of particular inductances for different configurations of the control windings. Figure 15 illustrates the results of the measurements.

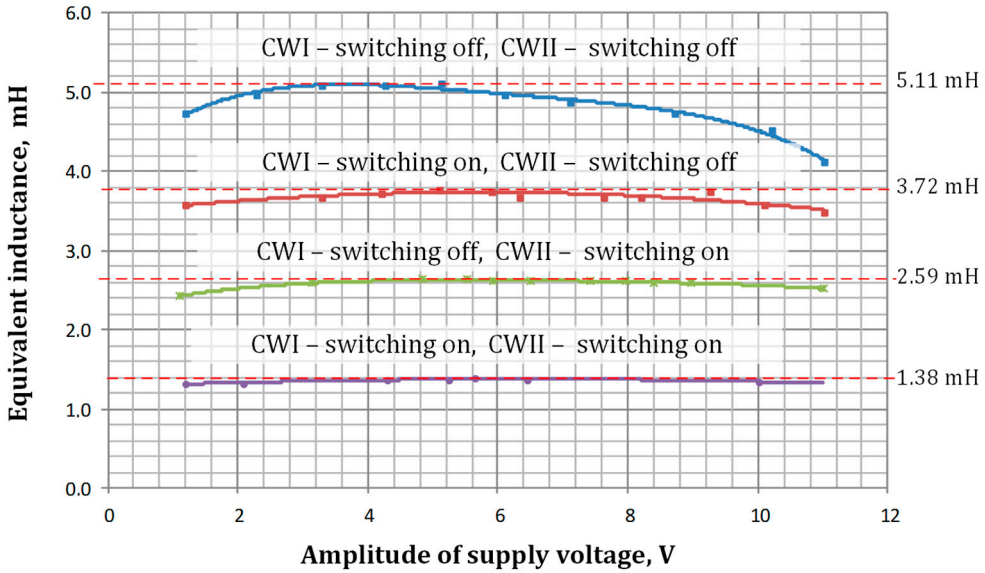

Figure 15. Measurement results for different supply voltages, CWI—control winding I, CWII—control winding II.

The comparison of inductance values obtained from optimization calculations, the three-dimensional FEM model and experimental measurements are presented in Table 5.

Table 5. Comparison of the optimization, simulation and experimental results.

	Assumed Value	Optimization	FEM Model	Prototype
L_1 [mH]	5.00	4.96	5.12	5.11
L_2 [mH]	3.75	3.77	3.88	3.72
L_3 [mH]	2.50	2.48	2.44	2.59
L_4 [mH]	1.25	1.24	1.29	1.38

The difference between assumed values of particular inductance and results optimization is small. The divergence in the case of L_1 inductance is about 1%.

The greatest diversity between the optimization and 3D simulation is obtained for L_1. The value of the relative error was approximately 3.3%. The largest difference between the device prototype and the optimization result is for the L_4 inductance and is approximately 10%, respectively.

The results of the conducted research show that the developed improved lumped parameter model can be successfully applied to the tuned inductive choke design process. The application of the lumped parameter model significantly shortens the optimization process total time and allows for calculations to be performed for a larger number of salps. The employment of a more accurate 3D model of the phenomena in the designed device slightly improves the accuracy of calculations (about 3.3%—see Table 5), but it significantly extends the total duration of the optimization process.

7. Conclusions

This paper presents the development of a mathematical model for a three-column tuned inductive choke and its integration into optimization software. The optimization process employed the salp swarm algorithm (SSA), a recent swarm intelligence method, adapted by modifying the a_1 characteristic SSA coefficient to better suit the optimization of the tuned inductive choke. After performing many test calculations, the value of the objective function described by the relationship (13) was adopted. The form of the objective function declared in this way provided the best repeatability of the results and reliability of the optimization procedure.

The results of the optimization calculation confirm that in order to obtain the expected relation between various inductances of the main winding, the software supporting the design process can be successfully applied.

The developed lumped parameter model is characterized by high accuracy. The accuracy of the developed model was verified using a three-dimensional field model. The application of the lumped model of the tuned inductive choke significantly speeds up optimization calculations. It is possible to employ a salp swarm with a large number of individual individuals, which allows for improving the probability of finding the global extremum with a single launch.

The developed algorithm and software can be successfully applied for the design of a series of products (tuned inductive chokes) for different supply voltages and different values of inductance for main winding.

Based on the results of the optimization calculations, simulation calculations were performed using a 3D model in CST Studio Suite. The results of field calculations confirm the good accuracy of the lumped parameter model and the reliability of the optimization procedure.

In order to evaluate the research work carried out using the optimization procedure, a prototype of the device was constructed. The dimensions were selected based on the results of optimization calculations.

As a result of the comparison, a high degree of convergence between the results of optimization, simulation calculations and the experimental results were obtained.

The developed optimization software should be applied for the optimal design of tuned inductive chokes, particularly when the ferromagnetic core does not exhibit significant saturation.

In future research, the authors intend to apply another algorithm from a group of nature-inspired optimization algorithms to compare results and convergences with SSA groups. Additionally, the authors plan to perform optimization of the tuned inductive choke containing three control winding.

Author Contributions: Conceptualization, Ł.K. and R.W.; methodology, M.K., Ł.K. and R.W.; software, R.W. and Ł.K.; formal analysis, M.K.; investigation, M.G. and R.W.; data curation, Ł.K.; writing—original draft preparation, Ł.K. and M.K.; writing—review and editing, R.W. and M.G. All authors have read and agreed to the published version of the manuscript.

Funding: This research was funded by the Polish Government, grant number 0212/SBAD/0594.

Data Availability Statement: The original contributions presented in the study are included in the article, further inquiries can be directed to the corresponding author.

Conflicts of Interest: The authors declare no conflicts of interest.

References

1. Gauthey, T.; Hassan, M.H.; Messine, F.; Gillon, F. Topology Optimization of the Harmonic Content for Torque Ripple Minimization. *IEEE Trans. Magn.* **2024**, *60*, 1–4. [CrossRef]
2. Zhou, Z.; He, Z.; Xue, G.; Zhou, J.; Rong, C.; Liu, G. Analysis of Magnetic Field Characteristics of a Giant Magnetostrictive Actuator with a Semi-Closed Magnetic Circuit. *Actuators* **2022**, *11*, 108. [CrossRef]
3. Knypiński, Ł. Constrained optimization of line-start PM motor based on the gray wolf optimizer. *Eksploat. I Niezawodn.* **2021**, *23*, 1–10. [CrossRef]
4. Mociran, B.; Topa, V. The Optimization of the Interior Permanent Magnetic Motor Case Study. *Electronics* **2023**, *12*, 2982. [CrossRef]
5. Aydoun, R.; Parent, G.; Tounzi, A.; Lecointe, J. Performance comparison of axial-flux switched reluctance machines with non-oriented and grain-oriented electrical steel rotors. *Open Phys.* **2020**, *18*, 981–988. [CrossRef]
6. Qu, C.; Guo, Z.; Hu, Y.; Wang, X.; Han, F. Multi-Objective Optimization Design of a New Permanent Magnet Synchronous Motor Based on the Taguchi Method. *Energies* **2022**, *15*, 7347. [CrossRef]
7. Alim Ritonga, S.; Sah Putra Sidauruk, I.; Herianto; Christofer Sitanggang, A. Analysis and Comparison of 3D Printed Soft Pneumatic Actuator Configurations for Swaying Lateral Motion of Planar Objects. *J. Inotera* **2024**, *9*, 67–75. [CrossRef]
8. Fu, D.; Jia, Z.; Xu, Y.; Gong, J.; Gillon, F.; Bracikowski, N.; Wu, X. Optimization design of a novel flux-switching transverse-flux permanent magnet tube linear motor. *IEEE Trans. Magn.* **2021**, *57*, 1–5. [CrossRef]
9. Tomar, V.; Bansal, M.; Singh, P. Metaheuristic Algorithms for Optimization: A Brief Review. *Eng. Proc.* **2023**, *59*, 238. [CrossRef]

10. Elio, J.; Peinado-Guerrero, M.; Villalobos, R.; Milcarek, R. An energy storage dispatch optimization for demand-side management in industrial facilities. *J. Energy Storage* **2022**, *53*, 105063. [CrossRef]
11. Knypiński, Ł.; Devarapalli, R.; Gillon, F. The hybrid algorithms in constrained optimization of the permanent magnet motors. *IET Sci. Meas. Technol.* **2024**, *1*, 1–7. [CrossRef]
12. Mutluer, M.; Şahman, M.A.; Çunkaş, M. Heuristic Optimization Based on Penalty Approach for Surface Permanent Magnet Synchronous Machines. *Arab. J. Sci. Eng.* **2020**, *45*, 6751–6767. [CrossRef]
13. Amiri, M.H.; Mehrabi Hashjin, N.; Montazeri, M.; Mirjalili, S. Hippopotamus optimization algorithm: A novel nature-inspired optimization algorithm. *Sci. Rep.* **2024**, *14*, 5032. [CrossRef] [PubMed]
14. Gharehchopogh, F.S.; Namazi, M.; Ebrahimi, L.; Abdollahzadeh, B. Advances in Sparrow Search Algorithm: A Comprehensive Survey. *Arch. Comput. Methods Eng.* **2023**, *30*, 427–455. [CrossRef]
15. Yang, C.; Wu, T.; Zeng, L. Enhancing the chimp optimization algorithm to evolve deep LSTMs for accounting profit prediction using adaptive pair reinforced technique. *Evol. Syst.* **2024**, *15*, 1159–1178. [CrossRef]
16. Zhang, Q.; Du, S.; Zhang, Y.; Wu, H.; Duan, K.; Lin, Y. A Novel Chimp Optimization Algorithm with Refraction Learning and Its Engineering Applications. *Algorithms* **2022**, *15*, 189. [CrossRef]
17. Gwóźdź, M.; Wojciechowski, R.M. Possibility of using a tuned inductor in a power device to improve the quality of electricity. *Arch. Electr. Eng.* **2022**, *71*, 1065–1080.
18. Ou, Y.; Yin, P.; Mo, L. An Improved Grey Wolf Optimizer and Its Application in Robot Path Planning. *Biomimetics* **2023**, *8*, 84. [CrossRef]
19. Kindl, V.; Sobotka, L.; Frivaldsky, M.; Skalicky, M. Analytical Method for Designing Three-Phase Air-Gapped Compensation Choke. *Energies* **2022**, *15*, 7328. [CrossRef]
20. Saini, D.; Ayachit, A.; Reatti, A.; Kazimierczuk, M.K. Analysis and Design of Choke Inductors for Switched-Mode Power Inverters. *IEEE Trans. Ind. Electron.* **2018**, *65*, 2234–2244. [CrossRef]
21. Zhang, X.; Xiao, F.; Wang, R.; Fan, X.; Wang, H. Improved calculation method for inductance value of the air-gap inductor. In Proceedings of the IEEE China International Youth Conference on Electrical Engineering (CIYCEE), Wuhan, China, 1–4 November 2020; pp. 1–6.
22. Kulkarni, S.; Khaparde, S. *Transformer Engineering: Design and Practice*; Marcel Dekker, Inc.: New York, NY, USA, 2004.
23. Mirjalili, S.; Gandomi, A.H.; Zahra Mirjalili, S.; Saremi, S.; Faris, H.; Mohammad Mirjalili, S. Salp Swarm Algorithm: A bio-inspired optimizer for engineering design problems. *Adv. Eng. Softw.* **2017**, *114*, 1–29. [CrossRef]
24. Wasim, S.M.; Amjad, M.; Habib, S.; Abbasi, A.M.; Bhatti, R.A.; Muyeen, S.M. A critical review and performance comparisons of swarm-based optimization algorithms in maximum power point tracking of photovoltaic systems under partial shading conditions. *Energy Rep.* **2022**, *8*, 4871–4898. [CrossRef]
25. Castelli, M.; Manzoni, L.; Mariot, L.; Nobile, M.; Tangherloni, A. Salp Swarm Optimization: A critical review. *Expert Syst. Appl.* **2022**, *189*, 116029. [CrossRef]
26. Khajehzadeh, M.; Iraji, A.; Majdi, A.; Keawsawasvong, S.; Nehdi, M.L. Adaptive Salp Swarm Algorithm for Optimization of Geotechnical Structures. *Appl. Sci.* **2022**, *12*, 6749. [CrossRef]
27. Wang, R.; Li, K.; Ming, Y.; Guo, W.; Deng, B.; Tang, H. An enhanced salp swarm algorithm with chaotic mapping and dynamic learning for optimizing purge process of proton exchange membrane fuel cell systems. *Energy* **2024**, *308*, 132852. [CrossRef]
28. Zivkovic, M.; Stoean, C.; Chhabra, A.; Budimirovic, N.; Petrovic, A.; Bacanin, N. Novel Improved Salp Swarm Algorithm: An Application for Feature Selection. *Sensors* **2022**, *22*, 1711. [CrossRef]
29. Herwan Sulaiman, M.; Mustaffa, Z. An application of improved salp swarm algorithm for optimal power flow solution considering stochastic solar power generation. *Adv. Electr. Eng. Electron. Energy* **2023**, *5*, 100195. [CrossRef]
30. Jia, F.; Luo, S.; Yin, G.; Ye, Y. A Novel Variant of the Salp Swarm Algorithm for Engineering Optimization. *J. Artif. Intell. Soft Comput. Res.* **2023**, *13*, 131–149. [CrossRef]